Preface

Modifications are shown in red.

Leukotriene B_4 promotes neovascularization and macrophage recruitment in murine wet-type AMD models

Fumiyuki Sasaki[1], Tomoaki Koga[1,2], Mai Ohba[1], Kazuko Saeki[1], Toshiaki Okuno[1], Keijiro Ishikawa[3], Takahito Nakama[3], Shintaro Nakao[3], Shigeo Yoshida[3], Tatsuro Ishibashi[3], Hamid Ahmadieh[4], Mozhgan Rezaei Kanavi[5], Ali Hafezi-Moghadam[6], Josef M. Penninger[7], Koh-Hei Sonoda[3] and Takehiko Yokomizo[1,*]

[1]Department of Biochemistry, Juntendo University School of Medicine, Tokyo, Japan.

[2]Current Address: Department of Medical Cell Biology, Institute of Molecular Embryology and Genetics, Kumamoto University, Kumamoto, Japan.

[3]Department of Ophthalmology, Graduate School of Medical Sciences, Kyushu University, Fukuoka, Japan.

[4]Ophthalmic Research Center, Shahid Beheshti University of Medical Sciences, Tehran, Iran.

[5]Ocular Tissue Engineering Research Center, Shahid Beheshti University of Medical Sciences, Tehran, Iran.

[6]Molecular Biomarkers Nano-Imaging Laboratory, Brigham & Women's Hospital, and Department of Radiology, Harvard Medical School, Boston, MA, USA.

[7]Institute of Molecular Biotechnology of the Austrian Academy of Sciences (IMBA), Vienna, Austria.

*Correspondence to Takehiko Yokomizo

Department of Biochemistry, Juntendo University School of Medicine.

Hongo 2-1-1, Bunkyo-ku, Tokyo 113-8421, Japan.

Telephone: +81-3-5802-1030 (office), 1031 (laboratory)

Fax: +81-3-5802-5889

E-mail: yokomizo-tky@umin.ac.jp

ORCID: 0000-0002-5219-1553

COI: The authors have declared that no conflict of interest exists except for the U.S. patent application No 15/525,660 (Fumiyuki Sasaki and Takehiko Yokomizo).

Running title: LTB_4-BLT1 axis exacerbates laser-induced CNV

Abbreviations:

5-LO, 5-lipoxygenase

AMD, age-related macular degeneration

BLT1, leukotriene B_4 receptor 1

BLT2, leukotriene B_4 receptor 2

CNV, choroidal neovascularization

FLAP, 5-lipoxygenase-activating protein

IVI, intravitreal injection

LTA_4H, leukotriene A_4 hydrolase

LTB_4, leukotriene B_4

RPE, retinal pigment epithelium

ABSTRACT

Age-related macular degeneration (AMD), a progressive chronic disease of the central retina, is associated with aging and is a leading cause of blindness worldwide. Here, we demonstrate that leukotriene B_4 (LTB_4) receptor 1 (BLT1) promotes laser-induced choroidal neovascularization (CNV) in a mouse model for wet-type AMD. CNV was significantly less in BLT1-deficient (BLT1-KO) mice compared to BLT1-WT controls. Expression of several pro-angiogenic and pro-fibrotic factors was lower in BLT1-KO eyes than in BLT1-WT eyes. LTB_4 production in the eyes was substantially increased in the early phase after laser injury. BLT1 was highly expressed in M2 macrophages *in vitro* and *in vivo*, and ocular $BLT1^+$ M2 macrophages were increased in the aged eyes post-laser injury. Furthermore, M2 macrophages were rapidly attracted by LTB_4 and subsequently produced VEGF-A through BLT1-mediated signaling. Consequently, intravitreal injection of M2 macrophages augmented CNV formation, which was attenuated by BLT1 deficiency. Thus, laser-induced injury to the retina triggered LTB_4 production and attracted M2 macrophages via BLT1, leading to development of CNV. A selective BLT1 antagonist (CP105696) and three LTB_4 inhibitors (Zileuton, MK-886, and Bestatin) reduced CNV in a dose-dependent manner. CP105696 also inhibited the accumulation of $BLT1^+$ M2 macrophages in the laser-injured eyes of aged mice. Together, these results indicate that the LTB_4-BLT1 axis is a novel therapeutic target for CNV of wet-type AMD.

Brief summary

Leukotriene B_4 attracts M2 macrophages and exacerbates laser-induced choroidal neovascularization. Leukotriene B_4 receptor 1 will be a novel target in the wet-type of

73 age-related macular degeneration.

INTRODUCTION

Age-related macular degeneration (AMD) is a chronic disease of the eye that is a leading cause of irreversible blindness in people over 50 years-of-age. AMD, which affects nearly 40 million individuals worldwide (1), is caused by deterioration of the retina, including the macula, which contains neuronal cells, photoreceptors, and retinal pigment epithelium (RPE) cells. AMD is classified as either wet (also called neovascular or exudative) type or dry (also called geographic atrophy) type. Wet AMD is characterized by degeneration of the macula, accompanied by fluid leakage from choroidal neovessels that have invaded the retina. The lesion is infiltrated by immune cells such as macrophages, DC, microglial cells, and T cells (e.g., NKT and γδT cells) (2-4). The main treatments for wet AMD are agents that inhibit VEGF; however, such agents frequently require repeated intravitreal injection (IVI), which can cause infectious endophathalmitis, intraocular inflammation, and ocular hemorrhage (5).

Leukotriene B_4 (LTB_4) receptor 1 (BLT1) is a G protein-coupled receptor (6) for a chemotactic eicosanoid, LTB_4 (7, 8), which is generated from arachidonic acid by 5-lipoxygenase (5-LO), 5-lipoxygenease-activating protein (FLAP), and LTA_4 hydrolase (LTA_4H) (9) (Supplemental Figure 1). BLT1 is expressed by various leukocyte subsets, including granulocytes (neutrophils and eosinophils), monocytes, macrophages, DC, differentiated T cells (Th1, Th2, Th17, and effector $CD8^+$ T cells), mast cells, and osteoclasts (10). As shown by previous reports, the LTB_4-BLT1 axis regulates inflammatory and immunological responses such as peritonitis (11), bronchial asthma (12, 13), delayed-type hypersensitivity (14), arthritis (15), atherosclerosis (16, 17), multiple sclerosis (18), psoriasis (19), and obesity-associated insulin resistance (20).

Activated macrophages are roughly classified as “classically activated” (M1-type) or

98 "alternatively activated" (M2-type) (21). M1 macrophages are induced by pathogen-
99 associated molecular patterns (e.g., LPS) and inflammatory cytokines (e.g., IFN-γ) and
100 defend against invading microbial pathogens such as bacteria, protozoa, and viruses.
101 Several proteins are used as markers to distinguish M1 and M2 macrophages. Inducible
102 NOS (iNOS) is a representative M1 marker (22-25), and co-stimulatory molecules (CD80
103 and CD86) and MHC class II are also useful markers for M1 polarization (26-30). M2
104 macrophages are regulated by Th2 cytokines (e.g., IL-4 and IL-13), anti-inflammatory
105 cytokines (e.g., IL-10 and TGF-β), immune complexes, glucocorticoids and other factors
106 (31) and are involved in diverse chronic inflammatory diseases such as parasite infections
107 (32), allergies (33), obesity (34, 35), and the pro-angiogenic responses that occur in cancer
108 (36) and tissue remodeling and repair (37-39). Mannose receptor (MR, CD206),
109 macrophage galactose N-acetyl-glactosamine specific lectin, (Mgl, CD301), programmed
110 cell death 1 ligand 2 (PD-L2, CD273), and PD-L1 (CD274) are well-characterized as the
111 cell surface markers (40-44), and Arginase-1, Fizz1, and Ym1 are known as distinct
112 markers (45-48) for M2 polarization. Recently, we and others reported that M2
113 macrophages recruited to the injured retina make a critical contribution to the
114 pathogenesis of choroidal neovascularization (CNV) in wet AMD (49-53); however, the
115 molecular mechanisms underlying recruitment of M2 macrophages are poorly
116 understood. Here, we show that BLT1 is mainly expressed by M2 macrophages, which
117 are then recruited to laser-induced retinal lesions and produced VEGF-A in a BLT1-
118 dependent manner. We also show that LTB_4-BLT1 signaling exacerbates CNV in a mouse
119 model of wet AMD by increasing expression of pro-angiogenic and pro-fibrotic markers.
120 Importantly, we confirm that blockade of LTB_4-BLT1 signaling strongly inhibits CNV.

RESULTS

BLT1 deficiency ameliorates progression of CNV in a mouse model of AMD

Recent reports showed that LTB_4-BLT1 signaling promotes several chronic diseases including fibrosis (54), insulin resistance (55), tumorigenesis (56); however, its role in chronic eye diseases has been poorly understood. To examine the pathological role of BLT1 in the eye *in vivo*, we performed retinal laser photocoagulation to induce wet AMD (57) in BLT1-WT and BLT1-deficient (BLT1-KO) mice (13) of various ages. BLT1-WT mice showed an age-dependent increase in CNV volume (Figure 1A, upper panels). Surprisingly, aging did not affect CNV development in BLT1-KO mice, and the volume of CNV was much smaller in old BLT1-KO mice than in old BLT1-WT mice (Figure 1A, lower panels). The CNV volume in BLT1-WT mice increased in an age-dependent manner (average volume in young mice, 3.1×10^5 μm^3; middle-aged mice, 5.4×10^5 μm^3; and old mice, 7.2×10^5 μm^3); this was not the case in BLT1-KO mice on Day 7 post-injury (young mice, 2.6×10^5 μm^3; middle-aged mice, 2.3×10^5 μm^3; and old mice, 3.2×10^5 μm^3) (Figure 1B). We also observed that the size of the laser-induced lesion in old BLT1-KO mice was smaller than that in old BLT1-WT mice (Figure 1C, lower panels); however, the overall retinal structure was the same in both groups (Figure 1C, upper panels). We also confirmed that BLT1-KO mice had smaller lesion areas than those of BLT1-WT mice in aged eyes (average area in BLT1-WT mice, 3.0×10^4 μm^2; BLT1-KO mice, 1.3×10^4 μm^2) (Figure 1D). In wet AMD, pathological angiogenesis is critically involved in CNV development and accelerates subretinal fibrosis by increasing various cytokines and chemokines (2, 58, 59). Consistently, expression of mRNA encoding pro-angiogenic growth factors *Vegfa*, *Pdgfb*, and *Fgf2* in laser-injured BLT1-KO eyes was approximately half as much as in BLT1-WT eyes on Day 7 post-laser injury in old mice

(Figure 2A, upper panels). The amounts of mRNA encoding inflammatory cytokines (*Il1b* and *Tnf*), endothelial cell markers (*Tek,* also known as *Tie2*, and *Vwf*), and the pro-fibrotic factors *Tgfb1*, *Pdgfb*, and *Fgf2* (59) were lower in laser-treated BLT1-KO eyes. However, expression of mRNA encoding the chemokines *Ccl3* (Figure 2A, middle and lower panels) and *Ccl2* (data not shown), both of which were reported to play a role in AMD pathogenesis (60, 61), was not significantly different between the BLT1-KO and BLT-WT groups. We previously cloned a low-affinity LTB_4 receptor, BLT2 (62, 63), which is involved in colitis (64), epidermal wound healing (65), and acute lung injury (66), and examined the effect of BLT2 deficiency in the same AMD model (Supplemental Figure 2). We found that BLT2 was not involved in AMD because the CNV volume in BLT2-deficient (BLT2-KO) mice was comparable with that in their WT (BLT2-WT) littermates (BLT2-WT mice, 4.4×10^5 μm^3; BLT2-KO mice, 3.4×10^5 μm^3) (Supplemental Figure 2B). Next, we performed the simultaneous quantification of 52 eicosanoids in laser-injured mouse eyes using a LC-MS/MS (Figure 2 and Supplemental Figure 3). On Day 1 and Day 3 post-laser injury, the amount of LTB_4 (Figure 2B) and 5-hydroxyeicosatetraenoic acid (5-HETE) (Supplemental Figure 3A) in the eyes markedly increased both in young and old mice. These results are consistent with the previous studies showing that various leukotrienes including LTB_4 were produced from the retinal glial cells, retinal endothelial cells, and RPE in the pathogenesis of inflammatory eye diseases at early phase (67, 68). Taken together, these results suggest that LTB_4-BLT1 signaling is critical for progression of laser-induced CNV.

BLT1 is expressed by macrophages and is involved in CNV development

As BLT1 is highly expressed in various subsets of leukocytes, we speculated that BLT1

expressed in retinal leukocytes is responsible for CNV. Previous studies showed that retinal leukocytes were reconstituted with donor leukocytes by bone marrow (BM) transplantation (69-73). To examine whether BLT1-expressing leukocytes play a role in laser-induced CNV, we implanted BLT1-WT or BLT1-KO BM cells from aging donors into lethally irradiated WT mice from aging recipients to generate BM chimeric mice and then examined CNV volume (Figure 3, A and B). We confirmed that more than 90% of BM cells and peripheral blood leukocytes (PBL) of the CD45.2-positive ($CD45.2^+$) recipients (C57BL/6J-Ly5.2 mice) were donor-derived $CD45.1^+$ cells from a congenic strain (C57BL/6-Ly5.1 mice) (Supplemental Figure 4, A and B). These results showed that the efficiency of BM transplantation is independent of the age of donors or recipients (Supplemental Figure 4C). The volume of CNV in BLT1-KO chimeras was significantly smaller than that in BLT1-WT chimeras (BLT1-WT BM into WT, 10.3×10^5 μm^3; BLT1-KO BM into WT, 6.8×10^5 μm^3) (Figure 3B). We further analyzed the numbers and the percentages of leukocyte populations in the eyes by FACS analysis (Figure 3, C and D). $CD45^+$ total leukocytes and CD11b-high ($CD11b^{hi}$) F4/80-negative ($F4/80^-$) $Ly6G^{hi}$ neutrophils peaked at day 1, but $CD11b^{hi}$ $F4/80^-$ $Ly6C^{hi}$ inflammatory monocytes and $CD11b^{hi}$ $F4/80^{hi}$ macrophages peaked at day 3 after laser injury in the eyes of aged WT mice. Consistent with the previous studies, we found that BLT1 is abundantly expressed in $CD11b^{hi}$ $F4/80^-$ $Ly6G^{hi}$ neutrophils and $CD11b^{hi}$ $F4/80^{hi}$ macrophages in the laser-injured eyes (data not shown). We further observed that $BLT1^+$ macrophages infiltrated the periphery of the laser-injured area in the RPE-choroid in aged mice on Day 5 post-laser injury (Figure 3E, upper panels), but not in young mice (Figure 3E, lower panels). To determine whether $BLT1^+$ macrophages contribute to the development of CNV, we next depleted macrophages by IVI of clodronate liposomes (Figure 4 and Supplemental

193 Figure 5) as previously described (74). IVI of clodronate liposomes significantly reduced
194 F4/80$^+$ macrophages in the RPE-choroid compared to control liposomes (Supplemental
195 Figure 5C), but did not affect the number of DAPI$^+$ cells (Supplemental Figure 5D).
196 Macrophage depletion reduced CNV volume in BLT1-WT mice (control, 13.5×10^5 μm^3;
197 clodronate, 2.6×10^5 μm^3) to levels observed in BLT1-KO mice (control, 2.5×10^5 μm^3;
198 clodronate, 1.1×10^5 μm^3) (Figure 4B). Taken together, these results suggest that BLT1$^+$
199 macrophages exacerbate laser-induced CNV.
200
201 **BLT1 is expressed in M2 macrophages *in vitro* and *in vivo***
202 Recent studies have been shown that macrophages are skewed toward pro-angiogenic
203 phenotype in the injured tissue or the tumor microenvironment (36, 39, 44, 48, 53, 75).
204 Next, we examined BLT1 expression in M1 and M2 macrophages using BM-derived
205 macrophages (BMDMs) (Figure 5, A and B and Supplemental Figure 6A), RAW264.7
206 cells (mouse monocyte/macrophage cell line) (Figure 5C), and THP-1 cells (human
207 monocytic cell line) (Figure 5D). M2 polarization of BMDMs induced BLT1 mRNA
208 (Gene Symbol: *Ltb4r1*) (Figure 5A and Supplemental Figure 6A, M2) and protein (Figure
209 5B, M2) expression, while M1 polarization or non-polarized M0 BMDMs showed lower
210 levels of BLT1 expression (Figure 5, A and B and Supplemental Figure 6A, M0 and M1).
211 Polarization of BMDMs was confirmed by examining the expression levels of mRNA for
212 M2 specific markers including CD206 (*Mrc1*), CD301b (*Mgl2*), PD-L2 (*Pdcd1lg2*),
213 Arginase-1 (*Arg1*), Fizz1 (*Retnla*), and Ym1 (*Chil3*) (Supplemental Figure 6, B-G), or an
214 M1 specific marker, iNOS (*Nos2*) (Supplemental Figure 6H). Consistent with these
215 results, M2-polarization induced BLT1 expression in both RAW264.7 and THP-1 cells,
216 and M1- or M0-polarization did not (Figure 5, C and D, left panels). Expression of PD-

L2 and CD80 proteins also confirmed the proper M2 and M1 polarization, respectively (Figure 5, C and D, middle and right panels). In addition, we analyzed the number and percentage of M2 macrophages by FACS analysis (Figure 5, E-H). The absolute number of $CD206^+$ M2 macrophages peaked at day 3 after laser-injury (Figure 5E), but the percentage of $CD206^+$ M2 macrophages in $CD45^+$ total leukocytes (Figure 5F) or in $CD11b^{hi}$ $F4/80^{hi}$ total macrophages (Figure 5G) peaked at day 5 in the eyes of aged WT mice. The percentage of $BLT1^+$ $CD206^+$ M2 macrophages was significantly higher during Day 1 to Day 5 after laser injury in aged mice (Figure 5H). We also found that ocular-infiltrating $BLT1^+$ macrophages expressed high levels of several M2 markers (CD206, CD301, and PD-L2) on Day 5 post-laser injury (Figure 5I). Interestingly, the expression levels of the M2 markers on $BLT1^+$ macrophages were slightly higher than those on $BLT1^-$ macrophages (Figure 5I, lower panels). To note, we found that BLT1 expression (Figure 5, J and K) in aged mice were higher than those in young mice in the ocular-infiltrating $CD206^+$ M2 macrophages on Day 3 post-laser injury. These results suggest that the infiltration of ocular M2 macrophages is accelerated by age-dependent up-regulation of BLT1.

LTB_4-BLT1 axis up-regulates recruitment of M2 macrophages and subsequent VEGF-A production

Although some molecules and signaling pathway have been implicated in the activation of M2 macrophages, the cellular and molecular mechanism is not fully elucidated. In general, BLT1 mediates LTB_4-induced calcium mobilization, chemotaxis, and inhibition of adenyl cyclase through the activation of Gq and Gi proteins (76). To determine whether M2 macrophages express functional BLT1 *in vitro*, we performed calcium mobilization

241 (Figure 6A) and chemotaxis (Figure 6, B-D and Supplemental movie 1 and 2) assays.
242 M2-, but not M1- or M0-polarized RAW264.7 cells exhibited increased intracellular
243 calcium mobilization upon LTB_4 stimulation (Figure 6A) and migrated along an
244 increasing LTB_4 concentration gradient (Figure 6B and Supplemental movies 1 and 2).
245 The M2-RAW264.7 cells significantly responded to LTB_4 with a velocity and
246 directionality of 3.29 unit s^{-1} and 0.88, respectively (Figure 6, C and D). We next analyzed
247 the expression levels of VEGF-A mRNA (Figure 7A) and protein (Figure 7B) in M2
248 BMDMs from BLT1-WT and BLT1-KO mice. Stimulation of LTB_4 significantly induced
249 VEGF-A mRNA and protein expression in M2 BMDMs from BLT1-WT, but not in
250 BLT1-KO M2 BMDMs. Thus, LTB_4-BLT1 signal is important for activation of M2
251 macrophages.
252
253 **M2 macrophages promote BLT1-mediated development of CNV**
254 Recent findings have experimentally confirmed that adoptive transferred M2
255 macrophages develop CNV by stimulating an abnormal angiogenesis (52, 77-79). To
256 clarify whether $BLT1^+$ M2 macrophages exacerbate CNV, we adoptively transferred M0,
257 M1, and M2 macrophages from BLT1-WT or BLT1-KO mice into laser-injured WT mice
258 (Figure 8). Adoptive transfer of BLT1-WT M2-BMDMs resulted in marked CNV
259 formation when compared with transfer of BLT1-KO M2-BMDMs (BLT1-WT M2 into
260 WT, 10.5×10^5 μm^3; BLT1-KO M2 into WT, 4.4×10^5 μm^3); adoptive transfer of M0-
261 and M1-BMDMs has little effect on CNV formation (BLT1-WT M0, 2.9×10^5 μm^3;
262 BLT1-KO M0, 2.1×10^5 μm^3; BLT1-WT M1, 2.7×10^5 μm^3; BLT1-KO M1, 1.6×10^5
263 μm^3) (Figure 8, A and B). Histological analysis revealed that BLT1-WT M2-injected eyes
264 developed more robust neovascularization in retinal and choroidal tissues than BLT1-KO

M2-injected eyes (BLT1-WT M2 into WT, 2.8×10^4 μm^2; BLT1-KO M2 into WT, 1.0×10^4 μm^2) (Figure 8, C and D). Thus, expression of BLT1 is required for M2-induced CNV.

Pharmacological inhibition of LTB_4-BLT1 signaling ameliorates CNV development

Several studies demonstrated that a BLT1 antagonist CP105696 completely blocked [^{3}H]-labeled LTB_4 binding (IC_{50} of 3.7 nM for human neutrophils) (80), calcium mobilization (0.1-1 μM for human neutrophils) (81), phagocytosis (1 μM for BMDMs) (82), and chemotaxis (0.1 μM for mouse peritoneal macrophages) (20) by antagonizing BLT1. To investigate whether blockade of LTB_4-BLT1 signaling (Supplemental Figure 1) (9, 83, 84) attenuates CNV, we treated mice by IVI of CP105696, prior to laser-induced injury (Figure 9, A and C, upper panels). We also tested the effects of three inhibitors of LTB_4-producing enzymes: Zileuton, a specific inhibitor of 5-LO; MK-886, a specific inhibitor of FLAP; and Bestatin, an inhibitor of LTA_4H (Figure 9A, lower panels, and Figure 9C, middle and lower panels). CP105696 caused a dose-dependent reduction in CNV volume (DMSO, 6.6×10^5 μm^3; CP105696, 0.2 pmol: 3.5×10^5 μm^3; 2 pmol: 2.0×10^5 μm^3; 20 pmol: 1.0×10^5 μm^3) (Figure 9B) and in CNV lesion area (DMSO, 3.5×10^4 μm^2; CP105696, 20 pmol: 1.6×10^4 μm^2) (Figure 9D). The CNV development was also inhibited by treatment with Zileuton, MK-886, or Bestatin (CNV volume: Zileuton, 2.8×10^5 μm^3; MK-886, 2.8×10^5 μm^3; Bestatin, 1.9×10^5 μm^3) (CNV lesion area: Zileuton, 1.3×10^4 μm^2; MK-886, 1.8×10^4 μm^2; Bestatin, 1.4×10^4 μm^2) (Figure 9, B and D). Moreover, we confirmed that CP105696 suppressed the infiltration of $CD206^+$ M2 macrophages and $BLT1^+$ $CD206^+$ M2 macrophages (Figure 9, E and F).

Given that some of these drugs are orally available, the LTB_4-BLT1 axis may become a novel therapeutic target for laser-induced CNV.

DISCUSSION

Here, we demonstrated that the volume of CNV in BLT1-WT mice, but not in BLT1-KO mice, increases in an age-dependent manner (Figure 1). A high-affinity LTB_4 receptor, BLT1, which was expressed in ocular-infiltrating macrophages (Figure 3E) was responsible for CNV (Figure 4 and 8). On the other hands, a low-affinity LTB_4 receptor, BLT2, which is ubiquitously expressed in human and mouse tissues (85) including cornea and conjunctiva (86) was not involved in laser injury-induced CNV, because there was no significant difference in CNV volume and histology between BLT2-WT and BLT2-KO mice (Supplemental Figure 2). As we reported recently, M2-type macrophages are important for the development of CNV after laser injury (53); here, we also demonstrated that ocular-infiltrating M2 macrophages contribute to CNV development via LTB_4-BLT1 signaling pathway. Indeed, laser-induced injury increased the amount of LTB_4 in the eyes (Figure 2B), which then attracted $BLT1^+$ M2 macrophages to the injured mouse retina (Figure 5, E-K). We also found that BLT1 is only induced during M2 polarization of mouse and human macrophages by IL-10, IL-4, IL-13, and TGF-β (Figure 5, A-D). Preliminary experiments with a STAT3 selective inhibitor suggest that, of these, the IL-10/JAK1/STAT3 signaling pathway is likely critical for induction of BLT1 expression (Supplemental Figure 7). Recent studies show that expression of IL-10 and M2 markers (e.g., CD163 and Arginase-1), but not M1 markers (e.g., IL-6 and TNF-α), is increased in senescent macrophages, thereby promoting CNV development (51, 52). Therefore, we expected that BLT1 expression is also increased in senescent M2 macrophages in the eyes of older mice. We actually found that the BLT1 expression of M2 macrophages in the older eyes is higher than that in the younger eyes after induction of laser injury (Figure 5, J and K). The elevated BLT1 could accelerate LTB_4-dependent recruitment of M2

macrophages to CNV lesions leading to the production of various pro-angiogenic factors, including VEGF-A through the activation of BLT1 (Figure 7). Such chain of events would also promote human CNV in wet AMD.

The findings presented herein might contribute to the development of novel anti-AMD drugs (Figure 9). Although anti-VEGF agents (e.g., Ranibizumab and Bevacizumab) are clinically and commercially available for wet AMD (87), several clinical trials have examined new therapeutic agents that targeting components of the VEGF (e.g., VEGF receptor tyrosine kinases) or other (e.g., PDGF) signaling pathways (88). To date, the LTB_4-BLT1 axis has not been examined in AMD. We speculate that agents that target the LTB_4-BLT1 axis might become useful treatment options for human patients with severe wet AMD. In fact, we examined the BLT1 expression in the diabetic human donor eyes (early progressive diabetic retinopathy, age 55, female) compared with non-diabetic human donor eyes (car accident, age 13, male) (data not shown). We found that $BLT1^+$ cells infiltrated into the periphery of the macular drusen, a common early sign of AMD, and choroidal capillaries in the RPE-choroid of diabetic human eyes, but not in non-diabetic human eyes. Recent studies showed that infiltrated macrophages exhibit M2-phenotype, which accelerate neovascularization to promote tissue repair in the injured retina of retinopathy (38, 79, 89, 90). Hence, the BLT1 may be a promising therapeutic target for CNV of several diseases including wet AMD. The 5-LO inhibitor Zileuton is clinically used as an anti-asthmatic drug worldwide (83), and the LTA_4H inhibitor Ubenimex (Bestatin) is a chemotherapy agent in Japan (84), with known safety profiles in both cases. This allows their potential off label use as therapeutic agents for wet AMD, thereby ensuring patient safety. In contrast, MK-886 and CP105696 are not used clinically; thus more effective and safe inhibitors of FLAP, and antagonists of BLT1, are

337 required.

338

339 In conclusion, LTB_4 is a key mediator that attracts M2 macrophages to the laser-injured
340 retinas via BLT1, thereby increasing the severity of CNV. Antagonists of BLT1 or
341 inhibitors of LTB_4 biosynthesis may become novel therapeutic agents to inhibit CNV of
342 wet AMD.

METHODS

Animals

BLT1-KO and BLT2-KO mice were generated as previously described (13, 64) and then backcrossed with C57BL/6J mice for more than 12 generations. Aged WT mice (C57BL/6J: > 20 weeks old) were purchased from Japan SLC (Shizuoka, Japan) or Kyudo (Saga, Japan). All mice were maintained in a filtered-air laminar-flow enclosure in a specific pathogen-free facility and given standard laboratory food and water.

Reagents

The selective BLT1 antagonist, CP105696, was from Pfizer (New York, NY, USA). Zileuton (a 5-LO inhibitor), MK-886 sodium salt hydrate (a FLAP inhibitor), and Bestatin hydrochloride (an inhibitor of aminopeptidases, including LTA_4H) were obtained from Sigma-Aldrich (St. Louis, MO, USA). LTB_4 was purchased from Cayman Chemical (Ann Arbor, MI, USA). Unless otherwise noted, all Abs and cytokines were purchased from BioLegend (San Diego, CA, USA) and Peprotech (Rocky Hill, CT, USA), respectively.

Laser-induced wet AMD model

Mice were anesthetized by intraperitoneal injection of ketamine (100 mg/kg) and xylazine (10 mg/kg), and the pupils were dilated by application of 0.2% tropicamide and 1% phenylephrine hydrochloride (Santen Pharmaceutical Co., Osaka, Japan). Using a 532 nm laser, a slit-lamp delivery system, and a slide glass as a contact lens, four spots (laser power, 200 mW; exposure time, 100 ms; hole size, 75 μm) were placed into each eye. After laser-induced injury and prior to administration of antagonists/inhibitors, the eyes were subjected to IVI of CP105696 (0.2–20 pmol), Zileuton (20 pmol), MK-886 (20

pmol), Bestatin (20 pmol), or DMSO (vehicle, 0.1%). The volume of the CNV lesions was measured in choroidal flat mounts on Day 7 post-injury. The anterior segment and retina were removed from the eyecup after fixation in 4% paraformaldehyde in PBS. The remaining RPE-choroid complex was dehydrated in methanol and stained with 7 μg/ml fluorescein-labeled iB4 (derived from Griffonia Simplicifolia Lectin I) (Vector Laboratories, Burlingame, CA, USA). After relaxing radial incisions, this complex was flat mounted using mounting medium (Thermo Fisher Scientific) and coverslips. Z-stack images were obtained using a confocal microscope (A1R$^+$; Nikon, Tokyo, Japan) and the CNV volume was analyzed on reconstructed three-dimensional images using NIS-Elements (Nikon).

Polarization of M1 and M2 macrophages

BM cells in the femur and tibia were collected from BLT1-WT and BLT1-KO mice (> 20 weeks old) and further differentiated in RPMI 1640 (Wako, Osaka, Japan) supplemented with 10% FCS, 100 U/ml penicillin, and 100 μg/ml streptomycin (P/S) into BMDMs by treatment with 50 ng/ml M-CSF for 3 days. RAW264.7 (a subclone from clone TIB-71) (ATCC, Manassas, VA, USA) and THP-1 (clone TIB-202) (ATCC) cell lines were maintained in RPMI 1640 supplemented with 10% FCS and P/S. BMDMs and RAW264.7 cells were polarized by exposure to 2 ng/ml mouse IFN-γ and 0.1 μg/ml LPS (Sigma-Aldrich) (M1) or 20 ng/ml IL-4, IL-10, and IL-13 (from mouse) and 2 ng/ml human TGF-β1 (R&D Systems, Minneapolis, MN, USA) (M2) during 48 h. THP-1 cells were stimulated with 150 nM PMA for 24 h and then polarized with 2 ng/ml human IFN-γ and 0.1 μg/ml LPS (M1) or 20 ng/ml IL-4, IL-10, and IL-13 (from human) and 2 ng/ml human TGF-β1 (M2) during 48 h. M0 macrophages were generated by culture in medium

without cytokines. All cells were cultured under standard conditions at 37°C and 5% CO_2 in a humidified atmosphere.

H&E staining

Eyes were removed, soaked in 10% buffered formalin solution, embedded in paraffin, sliced (10 μm thickness) using a microtone, and stained with H&E. Images were acquired under a light microscope (BZ-9000; Keyence, Osaka, Japan) and quantified the CNV lesion area using Image J (National Institute of Health, Bethesda, MD).

Quantitative RT-PCR

Eyecups (the remaining retina, choroid, and RPE from 1–2 eyes) and M0-, M1-, or M2-polarized BMDMs were prepared from BLT1-WT and BLT1-KO mice. For VEGF-A mRNA expression analysis, M2 BMDMs were stimulated with 500 nM LTB_4 or ethanol (as a vehicle control) for 0.5 h. All samples were treated with TRIzol reagent (Thermo Fisher Scientific, Waltham, MA, USA) to isolate RNA, according to the manufacturer's instructions. cDNA was synthesized from total RNA with reverse transcriptase and an optimized blend of oligo-dTs and random primers using an QuantiTect Reverse Transcription kit (Qiagen, Hilden, Germany) or qPCR RT Master Mix (Toyobo, Osaka, Japan). Target genes were amplified using a real-time PCR System (Roche, Basel, Switzerland or Thermo Fisher Scientific), DNA polymerase, SYBR Green I Dye (Thermo Fisher Scientific) and specific primers. Gene expression was normalized to 18S rRNA (*Rn18s*) using the ΔΔCT method. The sequences of the primers are as follows: *Vegfa*: Forward, 5'-actggaccctggctttactg-3' and Reverse, 5'-tctgctctccttctgtcgtg-3'; *Rn18s*: Forward, 5'-gcaattattccccatgaacg-3' and Reverse, 5'-gggacttaatcaacgcaagc-3'; *Pdgfb*:

Forward, 5’-cggcctgtgactagaagtcc-3’ and Reverse, 5’-gagcttgaggcgtcttgg-3’; *Fgf2*: Forward, 5’-cggctctactgcaagaacg-3’ and Reverse, 5’-tgcttggagttgtagtttgacg-3’; *Il1b*: Forward, 5’-tgtaatgaaagacggcacacc-3’ and Reverse, 5’-tcttctttgggtattgcttgg-3’; *Tnf*: Forward, 5’-tcttctcattcctgcttgtgg-3’ and Reverse, 5’-ggtctgggccatagaactga-3’; *Tek*: Forward, 5’-cataggaggaaacctgttcacc-3’ and Reverse, 5’-gcccccacttctgagctt-3’; *Vwf*: Forward, 5’-ccaaggagggtctgcaact-3’ and Reverse, 5’-aaaggaagactctggcaagcta-3’; *Tgfb1*: Forward, 5’-tggagcaacatgtggaactc-3’ and Reverse, 5’-cagcagccggttaccaag-3’; *Ccl3*: Forward, 5’-tgcccttgctgttcttctct-3’ and Reverse, 5’-gtggaatcttccggctgtag-3’; and *Ltb4r1*: Forward, 5’-ctcggaggtgtccagcac-3’ and Reverse, 5’-gacaggcaggtgtgtccttc-3’.

Liquid chromatography-mass spectrometry (LC-MS) analysis

Eyecups isolated from 5–6 eyes were frozen immediately in liquid nitrogen and stored at -80°C. Samples were homogenized in a tissue disrupter (Automill, Tokken, Chiba, Japan) and lipids were extracted by incubation in methanol overnight at -20°C followed by centrifuged at 5,000 × *g* for 5 min at 4°C. Supernatants were then mixed with 9 volumes of 0.1% formic acid in water, which included deuterium-labeled internal standards (Cayman Chemical). Diluted samples were loaded onto a solid-phase extraction cartridge (Waters, Milford, MA, USA) and washed serially with 0.1% formic acid in water, 15% methanol and 0.1% formic acid in water, 0.1% formic acid in water, and petroleum ether. After drying the cartridge, eicosanoids were eluted by centrifugation with 200 µl of 0.1% formic acid in methanol. For reverse phase-HPLC-MS/MS, a Shimadzu liquid chromatography system consisting of four LC-20AD pumps, a SIL-20AC autosampler, a CTO-20AC column oven, a FCV-12AH six-port switching valve, and a TSQ Quantum Ultra triple quadrupole mass spectrometer equipped with an electrospray ionization (ESI)

ion source (Thermo Fisher Scientific) were used (91, 92). An aliquot of each sample (50 μL) was injected into the trap column, an Opti-Guard Mini C18, at a total flow rate of 500 μL/min. Three minutes after sample injection, the valve was switched to introduce the trapped sample to the analytical column, a Capcell Pak C18 MGS3 (Shiseido, Tokyo, Japan). Separation of lipids was achieved by a linear gradient using water and acetonitrile containing 0.1% formic acid. The total flow rate was 120 μL/min, the column temperature was set at 46°C, and the LC column eluent was introduced directly into a TSQ Quantum Ultra. All compounds were analyzed in a negative ion polarity mode. Eicosanoids were quantified by multiple reaction monitoring (MRM). The MRM transitions monitored were *m/z* 335 → 195 for LTB_4, *m/z* 624 → 272 for LTC_4, *m/z* 495 → 177 for LTD_4, *m/z* 319 → 115 for 5-HETE, *m/z* 339 → 197 for $[^2H_4]LTB_4$, *m/z* 629 → 272 for $[^2H_5]LTC_4$, *m/z* 500 → 177 for $[^2H_5]LTD_4$, *m/z* 327 → 116 for $[^2H_8]$5-HETE. For accurate quantification, calibration curves were generated for each target eicosanoid using known reference standards and the same isotope-labeled internal standard. Automated peak detection, calibration, and calculation were carried out by the Xcalibur 1.2 software package (Thermo Fisher Scientific).

BM transplantation

BM cells were collected from the both femurs and tibiae of donor BLT1-WT and BLT1-KO (> 20 weeks old) and 10^7 cells were intravenously injected into lethally irradiated (10 Gy X-rays) male WT recipients (> 20 weeks old). At 28 days post-transplantation, mice were subjected to laser-induced retinal injury, followed by analysis of CNV development.

Immunofluorescence staining and analysis

RPE-choroid complexes were prepared from WT mice as described above and blocked with 5% BSA/0.5% Triton X-100 in PBS for 1 h, followed by staining with 10 µg/ml anti-BLT1 (clone 7A8; generated in-house) (93) and 5 µg/ml Alexa Fluor 647-labeled anti-F4/80 (clone BM8) mAbs. After washing with 0.1% Tween in PBS, tissues were incubated with HRP-labeled anti-mouse IgG (500-fold dilution) (Rockland Immunochemicals, Limerick, PA, USA), followed by Tyramide-Alexa Fluor 488 (100-fold dilution) (Thermo Fisher Scientific). Nuclei were stained with DAPI (5 µg/ml; Sigma-Aldrich). Samples were visualized under a confocal microscope ($A1R^{+}$; Nikon).

Flow cytometry analysis

BMDMs and RAW264.7 cells were collected in PBS/2 mM EDTA (pH 7.4) containing 2% FCS (FACS buffer). Fc receptors were then blocked with an anti-CD16/32 (5 µg/ml; 2.4G2) Ab (Fc blocker). BMDMs were stained with anti-F4/80-FITC (5 µg/ml; clone BM8), anti-CD11b-allophycocyanin (APC) (2.5 µg/ml; clone M1/70), and biotin-labeled anti-mouse BLT1 (5 µg/ml; clone 7A8; generated in-house) Ab (93) or mouse IgG_1 (5 µg/ml; Thermo Fisher Scientific/eBioscience, San Diego, CA, USA) (as an isotype control). RAW264.7 cells were stained with anti-mouse BLT1 (5 µg/ml; clone 7A8), anti-PD-L2 (2.5 µg/ml; clone TY25), anti-CD80 (2.5 µg/ml; clone 16-10A1), or isotype controls for biotin-labeled anti-mouse Abs. After washing with PBS/EDTA, cells were stained with R-phycoerythrin (PE)-conjugated Streptavidin (0.5 µg/ml; Thermo Fisher Scientific/eBioscience). THP-1 cells were collected in FACS buffer, blocked with human Fc blocker (Miltenyi Biotec, Bergisch Gladbach, Germany) and stained with anti-human BLT1 (diluted 1:20; clone 203/14F11) (R&D Systems), anti-PD-L2 (5 µg/ml; clone

24F.10C12), anti-CD80 (10 µg/ml; clone 2D10), or an isotype control for PE-labeled anti-human Abs. Cells were analyzed in a flow cytometer (FACSCalibur or LSRFortessa; Becton Dickinson, Franklin Lakes, NJ, USA). Eyecups were collected from 4–6 laser-injured eyes as follows: (i) young (8-12 weeks old) or aged (> 20 weeks old) WT mice, (ii) CP105696- (20 pmol/eye) and DMSO-injected WT mice (> 20 weeks old), and ocular-infiltrating cells were isolated using Collagenase D (Roche) in RPMI 1640 as previously described (94). Cells were then incubated with mouse Fc blocker, followed by staining with anti-CD45-FITC (2.5 µg/ml; clone 30-F11) (Becton Dickinson), anti-Ly6G-PE/Cy7 (2.5 µg/ml; clone 1A8), anti-Ly6C-APC/Cy7 (2.5 µg/ml; clone HK1.4), anti-F4/80-Brilliant Violet 421 (2.5 µg/ml; clone BM8), anti-CD11b-Brilliant Violet 510 (5 µg/ml; clone M1/70), and anti-mouse BLT1-APC (5 µg/ml; clone 7A8; generated in-house) Abs in addition to 2.5 µg/ml anti-PD-L2 (clone TY25), 10 µg/ml anti-CD301 (clone ER-MP23) (Bio-Rad Laboratories), 10 µg/ml anti-CD206 (clone MR5D3) biotin-conjugated Abs or isotype controls. Cells were washed and stained with 0.5 µg/ml Streptavidin-PE, and analyzed in a flow cytometer (FACSVerse; Becton Dickinson). For all experiments, dead cells were excluded after staining with 7AAD (Becton Dickinson).

Liposome-mediated depletion of macrophages

Aged BLT1-WT and BLT1-KO mice (> 20 weeks old) received an IVI of 90 µg clodronate liposomes (including 16 µg of clodronic acid; injection volume, 2 µl/eye) (Katayama Chemical Industries, Osaka, Japan) or control liposomes after laser-induced injury. RPE-choroid complexes were prepared as described above, stained with Alexa 647-labeled anti-F4/80 mAb or rat IgG_{2a} (as an isotype control), and then nuclei were visualized with DAPI. $F4/80^+$ macrophages and $DAPI^+$ cells per field were counted using

Image J.

Adoptive transfer of macrophages

Aged WT mice received M0, M1, and M2 BMDMs (10^5 cells in PBS/eye; injection volume, 2 μl/eye) from aged BLT1-WT or BLT1-KO mice (> 20 weeks old) via IVI after laser-induced injury.

Calcium mobilization assay

RAW264.7 cells were incubated for 60 min with HBSS-based loading buffer containing 20 mM HEPES (pH 7.4) (Thermo Fisher Scientific), 2.5 mM Probenecid (Sigma-Aldrich), 0.04% Pluronic F-127 (Thermo Fisher Scientific), and 4 μM Fluo 4-AM (Dojindo laboratories, Kumamoto, Japan). Cells were then washed with HEPES-based buffer, seeded into 96-well black plates (10^4 cells/well), and stimulated with 0.5–1000 nM LTB_4 or 2 μM Ionomycin. Assay plates were then analyzed using FlexStation 3 (Molecular Devices, Sunnyvale, CA).

TAXIScan chemotaxis assay

Chemotaxis of RAW264.7 cells toward 100 nM LTB_4 or ethanol (as a vehicle control) was monitored using TAXIScan-FL (Effector Cell Institute Frontier, Tokyo, Japan), as described previously (95). Phase-contrast sequential images were acquired at 1 min intervals for 45 mins and stacked using Image J. Chemotactic parameters (velocity and directionality) were analyzed with the Image J 'Manual Tracking' plug-in and the Image J 'Chemotaxis and Migration tools' plug-in.

ELISA

For VEGF-A protein expression analysis, culture media were collected in M2 BMDMs from BLT1-WT or BLT1-KO mice after stimulation with 500 nM LTB_4 or ethanol (as a vehicle control) for 4 h. VEGF-A was measured culture media using the Mouse VEGF Quantikine ELISA Kit (R&D Systems) according to the manufacturer's instructions.

Statistics

Data are expressed as the mean ± SEM of at least three independent mice or eyes. Two data sets were compared using 2-tailed Student's *t* test. Multiple comparisons were performed using 1-way ANOVA followed by Bonferroni's, Newman-Keuls, or Dunnett's *post hoc* test, and 2-way ANOVA followed by Bonferroni's *post hoc* test. *P* value of less than 0.05 was considered statistically significant. All statistical analyses were performed using Prism version 5.0 (GraphPad Software, La Jolla, CA).

Study approval

All animal studies and procedures were approved by the Ethics Committees on Animal Experimentation in Juntendo University (approval numbers 250224, 260166, 270161, 280167, and 290171). All the studies in this manuscript were carried out in accordance with approved guidelines and regulations.

AUTHOR CONTRIBUTIONS

F.S. and T.Y. designed all experiments. F.S., M.O., K.I., H.A., and M.R.K. performed the experiments. T.K., M.O., K.S., T.O., K.I., T.N., S.N., S. Y., T.I., H.A., M.R.K., A.H.M., J.M.P., K.H.S., and T.Y. helped acquiring and analyzing data. T.Y. performed conducting experiments. F.S., A.H.M., and T.Y. wrote the manuscript.

ACKNOWLEDGMENTS

This work was supported by Grants-in-Aid for Scientific Research (KAKENHI) from the Ministry of Education, Culture, Sports, Science, and Technology (MEXT) of the Japan Society for the Promotion of Science (JSPS) (grant numbers 22116001, 22116002, 15H05897, 15H05904, 15H04708, and 18H02627 to TY, 25860223, 15K19032 and 17K08664 to TK, 24590386, 15K08316, and 18K06923 to KS, 25460374, 16K08596 and 15KK0320 to TO) and by grants from the Naito Foundation, the Ono Medical Research Foundation, the Uehara Memorial Foundation, the Mitsubishi Foundation, and the Takeda Science Foundation. This study was supported in part by a Grant-in-Aid (S1311011 to TY) from the Foundation for Strategic Research Projects in Private Universities of the MEXT and by a grant from the Institute for Environmental and Gender-Specific Medicine. We thank the Research Center for Human Disease Modeling (Kyushu University), the Research Support Center of the Division of Molecular and Biochemical Research (Juntendo University), and the Imaging Core Laboratory, the Institute of Medical Science (The University of Tokyo) for technical support. We also thank Dr. Eiichi Hasegawa (Harvard Medical School, Boston, MA) and Dr. Akihiko Yoshimura (Keio University, Tokyo, Japan) for technical support of AMD model and BM transplantation, Dr. Takako Ichiki (California Institute of Technology, Pasadena, CA) for technical support of chemotaxis assay, Dr. Miki Honda (Juntendo University), Dr. Akira Matsuda (Juntendo University), and the members of our laboratory for advice and helpful discussion. The authors declare no competing financial interests.

REFERENCES

1. World Health Organization. Global data on visual impairment 2010. http://www.who.int/blindness/publications/globaldata/en/. WHO Web site. Accessed November 1, 2016.
2. Ambati J, Atkinson JP, and Gelfand BD. Immunology of age-related macular degeneration. *Nat Rev Immunol.* 2013;13(6):438-451.
3. Carr AJ, Smart MJ, Ramsden CM, Powner MB, da Cruz L, and Coffey PJ. Development of human embryonic stem cell therapies for age-related macular degeneration. *Trends Neurosci.* 2013;36(7):385-395.
4. Fritsche LG, Fariss RN, Stambolian D, Abecasis GR, Curcio CA, and Swaroop A. Age-related macular degeneration: genetics and biology coming together. *Annu Rev Genomics Hum Genet.* 2014;15:151-171.
5. Falavarjani KG, and Nguyen QD. Adverse events and complications associated with intravitreal injection of anti-VEGF agents: a review of literature. *Eye (Lond).* 2013;27(7):787-794.
6. Yokomizo T, Izumi T, Chang K, Takuwa Y, and Shimizu T. A G-protein-coupled receptor for leukotriene B4 that mediates chemotaxis. *Nature.* 1997;387(6633):620-624.
7. Afonso PV, Janka-Junttila M, Lee YJ, McCann CP, Oliver CM, Aamer KA, Losert W, Cicerone MT, and Parent CA. LTB4 is a signal-relay molecule during neutrophil chemotaxis. *Dev Cell.* 2012;22(5):1079-1091.
8. Lammermann T, Afonso PV, Angermann BR, Wang JM, Kastenmuller W, Parent CA, and Germain RN. Neutrophil swarms require LTB4 and integrins at sites of cell death in vivo. *Nature.* 2013;498(7454):371-375.

603 9. Nakamura M, and Shimizu T. Leukotriene receptors. *Chem Rev.*
604 2011;111(10):6231-6298.
605 10. Yokomizo T. Two distinct leukotriene B4 receptors, BLT1 and BLT2. *J Biochem.*
606 2015;157(2):65-71.
607 11. Tager AM, Dufour JH, Goodarzi K, Bercury SD, von Andrian UH, and Luster
608 AD. BLTR mediates leukotriene B(4)-induced chemotaxis and adhesion and plays
609 a dominant role in eosinophil accumulation in a murine model of peritonitis. *J*
610 *Exp Med.* 2000;192(3):439-446.
611 12. Tager AM, Bromley SK, Medoff BD, Islam SA, Bercury SD, Friedrich EB,
612 Carafone AD, Gerszten RE, and Luster AD. Leukotriene B4 receptor BLT1
613 mediates early effector T cell recruitment. *Nat Immunol.* 2003;4(10):982-990.
614 13. Terawaki K, Yokomizo T, Nagase T, Toda A, Taniguchi M, Hashizume K, Yagi T,
615 and Shimizu T. Absence of leukotriene B4 receptor 1 confers resistance to airway
616 hyperresponsiveness and Th2-type immune responses. *J Immunol.*
617 2005;175(7):4217-4225.
618 14. Toda A, Terawaki K, Yamazaki S, Saeki K, Shimizu T, and Yokomizo T.
619 Attenuated Th1 induction by dendritic cells from mice deficient in the leukotriene
620 B4 receptor 1. *Biochimie.* 2010;92(6):682-691.
621 15. Kim ND, Chou RC, Seung E, Tager AM, and Luster AD. A unique requirement
622 for the leukotriene B4 receptor BLT1 for neutrophil recruitment in inflammatory
623 arthritis. *J Exp Med.* 2006;203(4):829-835.
624 16. Subbarao K, Jala VR, Mathis S, Suttles J, Zacharias W, Ahamed J, Ali H, Tseng
625 MT, and Haribabu B. Role of leukotriene B4 receptors in the development of
626 atherosclerosis: potential mechanisms. *Arterioscler Thromb Vasc Biol.*

627 2004;24(2):369-375.
628 17. Back M, Bu DX, Branstrom R, Sheikine Y, Yan ZQ, and Hansson GK.
629 Leukotriene B4 signaling through NF-kappaB-dependent BLT1 receptors on
630 vascular smooth muscle cells in atherosclerosis and intimal hyperplasia. *Proc Natl*
631 *Acad Sci U S A.* 2005;102(48):17501-17506.
632 18. Kihara Y, Yokomizo T, Kunita A, Morishita Y, Fukayama M, Ishii S, and Shimizu
633 T. The leukotriene B4 receptor, BLT1, is required for the induction of
634 experimental autoimmune encephalomyelitis. *Biochem Biophys Res Commun.*
635 2010;394(3):673-678.
636 19. Sumida H, Yanagida K, Kita Y, Abe J, Matsushima K, Nakamura M, Ishii S, Sato
637 S, and Shimizu T. Interplay between CXCR2 and BLT1 facilitates neutrophil
638 infiltration and resultant keratinocyte activation in a murine model of imiquimod-
639 induced psoriasis. *J Immunol.* 2014;192(9):4361-4369.
640 20. Li P, Oh DY, Bandyopadhyay G, Lagakos WS, Talukdar S, Osborn O, Johnson A,
641 Chung H, Mayoral R, Maris M, et al. LTB4 promotes insulin resistance in obese
642 mice by acting on macrophages, hepatocytes and myocytes. *Nat Med.*
643 2015;21(3):239-247.
644 21. Pelegrin P, and Surprenant A. Dynamics of macrophage polarization reveal new
645 mechanism to inhibit IL-1beta release through pyrophosphates. *EMBO J.*
646 2009;28(14):2114-2127.
647 22. Sindrilaru A, Peters T, Wieschalka S, Baican C, Baican A, Peter H, Hainzl A,
648 Schatz S, Qi Y, Schlecht A, et al. An unrestrained proinflammatory M1
649 macrophage population induced by iron impairs wound healing in humans and
650 mice. *J Clin Invest.* 2011;121(3):985-997.

651 23. Xu H, Zhu J, Smith S, Foldi J, Zhao B, Chung AY, Outtz H, Kitajewski J, Shi C,
652 Weber S, et al. Notch-RBP-J signaling regulates the transcription factor IRF8 to
653 promote inflammatory macrophage polarization. *Nat Immunol.* 2012;13(7):642-
654 650.
655 24. Klug F, Prakash H, Huber PE, Seibel T, Bender N, Halama N, Pfirschke C, Voss
656 RH, Timke C, Umansky L, et al. Low-dose irradiation programs macrophage
657 differentiation to an iNOS(+)/M1 phenotype that orchestrates effective T cell
658 immunotherapy. *Cancer Cell.* 2013;24(5):589-602.
659 25. Lu G, Zhang R, Geng S, Peng L, Jayaraman P, Chen C, Xu F, Yang J, Li Q, Zheng
660 H, et al. Myeloid cell-derived inducible nitric oxide synthase suppresses M1
661 macrophage polarization. *Nat Commun.* 2015;6:6676.
662 26. Verreck FA, de Boer T, Langenberg DM, Hoeve MA, Kramer M, Vaisberg E,
663 Kastelein R, Kolk A, de Waal-Malefyt R, and Ottenhoff TH. Human IL-23-
664 producing type 1 macrophages promote but IL-10-producing type 2 macrophages
665 subvert immunity to (myco)bacteria. *Proc Natl Acad Sci U S A.*
666 2004;101(13):4560-4565.
667 27. Iwata Y, Bostrom EA, Menke J, Rabacal WA, Morel L, Wada T, and Kelley VR.
668 Aberrant macrophages mediate defective kidney repair that triggers nephritis in
669 lupus-susceptible mice. *J Immunol.* 2012;188(9):4568-4580.
670 28. Bayer C, Varani S, Wang L, Walther P, Zhou S, Straschewski S, Bachem M,
671 Soderberg-Naucler C, Mertens T, and Frascaroli G. Human cytomegalovirus
672 infection of M1 and M2 macrophages triggers inflammation and autologous T-
673 cell proliferation. *J Virol.* 2013;87(1):67-79.
674 29. Deng T, Lyon CJ, Minze LJ, Lin J, Zou J, Liu JZ, Ren Y, Yin Z, Hamilton DJ,

Reardon PR, et al. Class II major histocompatibility complex plays an essential role in obesity-induced adipose inflammation. *Cell Metab.* 2013;17(3):411-422.

30. Cucak H, Grunnet LG, and Rosendahl A. Accumulation of M1-like macrophages in type 2 diabetic islets is followed by a systemic shift in macrophage polarization. *J Leukoc Biol.* 2014;95(1):149-160.

31. Biswas SK, and Mantovani A. Macrophage plasticity and interaction with lymphocyte subsets: cancer as a paradigm. *Nat Immunol.* 2010;11(10):889-896.

32. Satoh T, Takeuchi O, Vandenbon A, Yasuda K, Tanaka Y, Kumagai Y, Miyake T, Matsushita K, Okazaki T, Saitoh T, et al. The Jmjd3-Irf4 axis regulates M2 macrophage polarization and host responses against helminth infection. *Nat Immunol.* 2010;11(10):936-944.

33. Egawa M, Mukai K, Yoshikawa S, Iki M, Mukaida N, Kawano Y, Minegishi Y, and Karasuyama H. Inflammatory monocytes recruited to allergic skin acquire an anti-inflammatory M2 phenotype via basophil-derived interleukin-4. *Immunity.* 2013;38(3):570-580.

34. Odegaard JI, Ricardo-Gonzalez RR, Goforth MH, Morel CR, Subramanian V, Mukundan L, Red Eagle A, Vats D, Brombacher F, Ferrante AW, et al. Macrophage-specific PPARgamma controls alternative activation and improves insulin resistance. *Nature.* 2007;447(7148):1116-1120.

35. Satoh T, Kidoya H, Naito H, Yamamoto M, Takemura N, Nakagawa K, Yoshioka Y, Morii E, Takakura N, Takeuchi O, et al. Critical role of Trib1 in differentiation of tissue-resident M2-like macrophages. *Nature.* 2013;495(7442):524-528.

36. Colegio OR, Chu NQ, Szabo AL, Chu T, Rhebergen AM, Jairam V, Cyrus N, Brokowski CE, Eisenbarth SC, Phillips GM, et al. Functional polarization of

699 tumour-associated macrophages by tumour-derived lactic acid. *Nature.*
700 2014;513(7519):559-563.
701 37. Shaul ME, Bennett G, Strissel KJ, Greenberg AS, and Obin MS. Dynamic, M2-
702 like remodeling phenotypes of CD11c+ adipose tissue macrophages during high-
703 fat diet--induced obesity in mice. *Diabetes.* 2010;59(5):1171-1181.
704 38. Marchetti V, Yanes O, Aguilar E, Wang M, Friedlander D, Moreno S, Storm K,
705 Zhan M, Naccache S, Nemerow G, et al. Differential macrophage polarization
706 promotes tissue remodeling and repair in a model of ischemic retinopathy. *Sci*
707 *Rep.* 2011;1:76.
708 39. Shechter R, Miller O, Yovel G, Rosenzweig N, London A, Ruckh J, Kim KW,
709 Klein E, Kalchenko V, Bendel P, et al. Recruitment of beneficial M2 macrophages
710 to injured spinal cord is orchestrated by remote brain choroid plexus. *Immunity.*
711 2013;38(3):555-569.
712 40. Huber S, Hoffmann R, Muskens F, and Voehringer D. Alternatively activated
713 macrophages inhibit T-cell proliferation by Stat6-dependent expression of PD-L2.
714 *Blood.* 2010;116(17):3311-3320.
715 41. Spite M, Hellmann J, Tang Y, Mathis SP, Kosuri M, Bhatnagar A, Jala VR, and
716 Haribabu B. Deficiency of the leukotriene B4 receptor, BLT-1, protects against
717 systemic insulin resistance in diet-induced obesity. *J Immunol.* 2011;187(4):1942-
718 1949.
719 42. Parsa R, Andresen P, Gillett A, Mia S, Zhang XM, Mayans S, Holmberg D, and
720 Harris RA. Adoptive transfer of immunomodulatory M2 macrophages prevents
721 type 1 diabetes in NOD mice. *Diabetes.* 2012;61(11):2881-2892.
722 43. Huang SC, Everts B, Ivanova Y, O'Sullivan D, Nascimento M, Smith AM, Beatty

W, Love-Gregory L, Lam WY, O'Neill CM, et al. Cell-intrinsic lysosomal lipolysis is essential for alternative activation of macrophages. *Nat Immunol.* 2014;15(9):846-855.

44. Shiraishi M, Shintani Y, Shintani Y, Ishida H, Saba R, Yamaguchi A, Adachi H, Yashiro K, and Suzuki K. Alternatively activated macrophages determine repair of the infarcted adult murine heart. *J Clin Invest.* 2016;126(6):2151-2166.

45. Liao X, Sharma N, Kapadia F, Zhou G, Lu Y, Hong H, Paruchuri K, Mahabeleshwar GH, Dalmas E, Venteclef N, et al. Kruppel-like factor 4 regulates macrophage polarization. *J Clin Invest.* 2011;121(7):2736-2749.

46. Arranz A, Doxaki C, Vergadi E, Martinez de la Torre Y, Vaporidi K, Lagoudaki ED, Ieronymaki E, Androulidaki A, Venihaki M, Margioris AN, et al. Akt1 and Akt2 protein kinases differentially contribute to macrophage polarization. *Proc Natl Acad Sci U S A.* 2012;109(24):9517-9522.

47. Han MS, Jung DY, Morel C, Lakhani SA, Kim JK, Flavell RA, and Davis RJ. JNK expression by macrophages promotes obesity-induced insulin resistance and inflammation. *Science.* 2013;339(6116):218-222.

48. Neves J, Zhu J, Sousa-Victor P, Konjikusic M, Riley R, Chew S, Qi Y, Jasper H, and Lamba DA. Immune modulation by MANF promotes tissue repair and regenerative success in the retina. *Science.* 2016;353(6294):aaf3646.

49. Nakao S, Noda K, Zandi S, Sun D, Taher M, Schering A, Xie F, Mashima Y, and Hafezi-Moghadam A. VAP-1-mediated M2 macrophage infiltration underlies IL-1beta- but not VEGF-A-induced lymph- and angiogenesis. *Am J Pathol.* 2011;178(4):1913-1921.

50. Horie S, Robbie SJ, Liu J, Wu WK, Ali RR, Bainbridge JW, Nicholson LB,

Mochizuki M, Dick AD, and Copland DA. CD200R signaling inhibits pro-angiogenic gene expression by macrophages and suppresses choroidal neovascularization. *Sci Rep.* 2013;3:3072.

51. Sene A, Khan AA, Cox D, Nakamura RE, Santeford A, Kim BM, Sidhu R, Onken MD, Harbour JW, Hagbi-Levi S, et al. Impaired cholesterol efflux in senescent macrophages promotes age-related macular degeneration. *Cell Metab.* 2013;17(4):549-561.

52. Nakamura R, Sene A, Santeford A, Gdoura A, Kubota S, Zapata N, and Apte RS. IL10-driven STAT3 signalling in senescent macrophages promotes pathological eye angiogenesis. *Nat Commun.* 2015;6:7847.

53. Zandi S, Nakao S, Chun KH, Fiorina P, Sun D, Arita R, Zhao M, Kim E, Schueller O, Campbell S, et al. ROCK-isoform-specific polarization of macrophages associated with age-related macular degeneration. *Cell Rep.* 2015;10(7):1173-1186.

54. Lv J, Xiong Y, Li W, Yang W, Zhao L, and He R. BLT1 Mediates Bleomycin-Induced Lung Fibrosis Independently of Neutrophils and CD4+ T Cells. *J Immunol.* 2017;198(4):1673-1684.

55. Ying W, Wollam J, Ofrecio JM, Bandyopadhyay G, El Ouarrat D, Lee YS, Oh DY, Li P, Osborn O, and Olefsky JM. Adipose tissue B2 cells promote insulin resistance through leukotriene LTB4/LTB4R1 signaling. *J Clin Invest.* 2017;127(3):1019-1030.

56. Bodduluri SR, Mathis S, Maturu P, Krishnan E, Satpathy SR, Chilton PM, Mitchell TC, Lira S, Locati M, Mantovani A, et al. Mast Cell-Dependent CD8(+) T-cell Recruitment Mediates Immune Surveillance of Intestinal Tumors in

771 Apc(Min/+) Mice. *Cancer Immunol Res.* 2018.

772 57. Lambert V, Lecomte J, Hansen S, Blacher S, Gonzalez ML, Struman I, Sounni
773 NE, Rozet E, de Tullio P, Foidart JM, et al. Laser-induced choroidal
774 neovascularization model to study age-related macular degeneration in mice. *Nat*
775 *Protoc.* 2013;8(11):2197-2211.

776 58. Ferrara N, Mass RD, Campa C, and Kim R. Targeting VEGF-A to treat cancer
777 and age-related macular degeneration. *Annu Rev Med.* 2007;58:491-504.

778 59. Ishikawa K, Kannan R, and Hinton DR. Molecular mechanisms of subretinal
779 fibrosis in age-related macular degeneration. *Exp Eye Res.* 2016;142:19-25.

780 60. Ambati J, Anand A, Fernandez S, Sakurai E, Lynn BC, Kuziel WA, Rollins BJ,
781 and Ambati BK. An animal model of age-related macular degeneration in
782 senescent Ccl-2- or Ccr-2-deficient mice. *Nat Med.* 2003;9(11):1390-1397.

783 61. Takeda A, Baffi JZ, Kleinman ME, Cho WG, Nozaki M, Yamada K, Kaneko H,
784 Albuquerque RJ, Dridi S, Saito K, et al. CCR3 is a target for age-related macular
785 degeneration diagnosis and therapy. *Nature.* 2009;460(7252):225-230.

786 62. Yokomizo T, Kato K, Terawaki K, Izumi T, and Shimizu T. A second leukotriene
787 B(4) receptor, BLT2. A new therapeutic target in inflammation and
788 immunological disorders. *J Exp Med.* 2000;192(3):421-432.

789 63. Okuno T, Iizuka Y, Okazaki H, Yokomizo T, Taguchi R, and Shimizu T. 12(S)-
790 Hydroxyheptadeca-5Z, 8E, 10E-trienoic acid is a natural ligand for leukotriene
791 B4 receptor 2. *J Exp Med.* 2008;205(4):759-766.

792 64. Iizuka Y, Okuno T, Saeki K, Uozaki H, Okada S, Misaka T, Sato T, Toh H,
793 Fukayama M, Takeda N, et al. Protective role of the leukotriene B4 receptor BLT2
794 in murine inflammatory colitis. *FASEB J.* 2010;24(12):4678-4690.

795 65. Liu M, Saeki K, Matsunobu T, Okuno T, Koga T, Sugimoto Y, Yokoyama C,
796 Nakamizo S, Kabashima K, Narumiya S, et al. 12-Hydroxyheptadecatrienoic acid
797 promotes epidermal wound healing by accelerating keratinocyte migration via the
798 BLT2 receptor. *J Exp Med.* 2014;211(6):1063-1078.
799 66. Shigematsu M, Koga T, Ishimori A, Saeki K, Ishii Y, Taketomi Y, Ohba M, Jo-
800 Watanabe A, Okuno T, Harada N, et al. Leukotriene B4 receptor type 2 protects
801 against pneumolysin-dependent acute lung injury. *Sci Rep.* 2016;6:34560.
802 67. Talahalli R, Zarini S, Sheibani N, Murphy RC, and Gubitosi-Klug RA. Increased
803 synthesis of leukotrienes in the mouse model of diabetic retinopathy. *Invest*
804 *Ophthalmol Vis Sci.* 2010;51(3):1699-1708.
805 68. Subramanian P, Mendez EF, and Becerra SP. A Novel Inhibitor of 5-Lipoxygenase
806 (5-LOX) Prevents Oxidative Stress-Induced Cell Death of Retinal Pigment
807 Epithelium (RPE) Cells. *Invest Ophthalmol Vis Sci.* 2016;57(11):4581-4588.
808 69. Espinosa-Heidmann DG, Caicedo A, Hernandez EP, Csaky KG, and Cousins SW.
809 Bone marrow-derived progenitor cells contribute to experimental choroidal
810 neovascularization. *Invest Ophthalmol Vis Sci.* 2003;44(11):4914-4919.
811 70. Kezic JM, and McMenamin PG. The effects of CX3CR1 deficiency and
812 irradiation on the homing of monocyte-derived cell populations in the mouse eye.
813 *PLoS One.* 2013;8(7):e68570.
814 71. Espinosa-Heidmann DG, Malek G, Mettu PS, Caicedo A, Saloupis P, Gach S,
815 Dunnon AK, Hu P, Spiga MG, and Cousins SW. Bone marrow transplantation
816 transfers age-related susceptibility to neovascular remodeling in murine laser-
817 induced choroidal neovascularization. *Invest Ophthalmol Vis Sci.*
818 2013;54(12):7439-7449.

819 72. Singh V, Jaini R, Torricelli AA, Tuohy VK, and Wilson SE. A method to generate
820 enhanced GFP+ chimeric mice to study the role of bone marrow-derived cells in
821 the eye. *Exp Eye Res.* 2013;116:366-370.
822 73. O'Koren EG, Mathew R, and Saban DR. Fate mapping reveals that microglia and
823 recruited monocyte-derived macrophages are definitively distinguishable by
824 phenotype in the retina. *Sci Rep.* 2016;6:20636.
825 74. Sakurai E, Anand A, Ambati BK, van Rooijen N, and Ambati J. Macrophage
826 depletion inhibits experimental choroidal neovascularization. *Invest Ophthalmol*
827 *Vis Sci.* 2003;44(8):3578-3585.
828 75. Zhou W, Ke SQ, Huang Z, Flavahan W, Fang X, Paul J, Wu L, Sloan AE,
829 McLendon RE, Li X, et al. Periostin secreted by glioblastoma stem cells recruits
830 M2 tumour-associated macrophages and promotes malignant growth. *Nat Cell*
831 *Biol.* 2015;17(2):170-182.
832 76. Kuniyeda K, Okuno T, Terawaki K, Miyano M, Yokomizo T, and Shimizu T.
833 Identification of the intracellular region of the leukotriene B4 receptor type 1 that
834 is specifically involved in Gi activation. *J Biol Chem.* 2007;282(6):3998-4006.
835 77. Bacci M, Capobianco A, Monno A, Cottone L, Di Puppo F, Camisa B, Mariani
836 M, Brignole C, Ponzoni M, Ferrari S, et al. Macrophages are alternatively
837 activated in patients with endometriosis and required for growth and
838 vascularization of lesions in a mouse model of disease. *Am J Pathol.*
839 2009;175(2):547-556.
840 78. Hughes R, Qian BZ, Rowan C, Muthana M, Keklikoglou I, Olson OC, Tazzyman
841 S, Danson S, Addison C, Clemons M, et al. Perivascular M2 Macrophages
842 Stimulate Tumor Relapse after Chemotherapy. *Cancer Res.* 2015;75(17):3479-

3491.

79. Zhou Y, Yoshida S, Nakao S, Yoshimura T, Kobayashi Y, Nakama T, Kubo Y, Miyawaki K, Yamaguchi M, Ishikawa K, et al. M2 Macrophages Enhance Pathological Neovascularization in the Mouse Model of Oxygen-Induced Retinopathy. *Invest Ophthalmol Vis Sci.* 2015;56(8):4767-4777.

80. Griffiths RJ, Pettipher ER, Koch K, Farrell CA, Breslow R, Conklyn MJ, Smith MA, Hackman BC, Wimberly DJ, Milici AJ, et al. Leukotriene B4 plays a critical role in the progression of collagen-induced arthritis. *Proc Natl Acad Sci U S A.* 1995;92(2):517-521.

81. Mathis SP, Jala VR, Lee DM, and Haribabu B. Nonredundant roles for leukotriene B4 receptors BLT1 and BLT2 in inflammatory arthritis. *J Immunol.* 2010;185(5):3049-3056.

82. Okamoto F, Saeki K, Sumimoto H, Yamasaki S, and Yokomizo T. Leukotriene B4 augments and restores Fc gammaRs-dependent phagocytosis in macrophages. *J Biol Chem.* 2010;285(52):41113-41121.

83. Funk CD. Leukotriene modifiers as potential therapeutics for cardiovascular disease. *Nat Rev Drug Discov.* 2005;4(8):664-672.

84. Wickstrom M, Larsson R, Nygren P, and Gullbo J. Aminopeptidase N (CD13) as a target for cancer chemotherapy. *Cancer Sci.* 2011;102(3):501-508.

85. Saeki K, and Yokomizo T. Identification, signaling, and functions of LTB4 receptors. *Semin Immunol.* 2017;33:30-36.

86. Iwamoto S, Koga T, Ohba M, Okuno T, Koike M, Murakami A, Matsuda A, and Yokomizo T. Non-steroidal anti-inflammatory drug delays corneal wound healing by reducing production of 12-hydroxyheptadecatrienoic acid, a ligand for

leukotriene B4 receptor 2. *Sci Rep.* 2017;7(1):13267.

87. Group CR, Martin DF, Maguire MG, Ying GS, Grunwald JE, Fine SL, and Jaffe GJ. Ranibizumab and bevacizumab for neovascular age-related macular degeneration. *N Engl J Med.* 2011;364(20):1897-1908.

88. Syed BA, Evans JB, and Bielory L. Wet AMD market. *Nat Rev Drug Discov.* 2012;11(11):827.

89. Gao S, Li C, Zhu Y, Wang Y, Sui A, Zhong Y, Xie B, and Shen X. PEDF mediates pathological neovascularization by regulating macrophage recruitment and polarization in the mouse model of oxygen-induced retinopathy. *Sci Rep.* 2017;7:42846.

90. Nakama T, Yoshida S, Ishikawa K, Kubo Y, Kobayashi Y, Zhou Y, Nakao S, Hisatomi T, Ikeda Y, Takao K, et al. Therapeutic Effect of Novel Single-Stranded RNAi Agent Targeting Periostin in Eyes with Retinal Neovascularization. *Mol Ther Nucleic Acids.* 2017;6:279-289.

91. Matsunobu T, Okuno T, Yokoyama C, and Yokomizo T. Thromboxane A synthase-independent production of 12-hydroxyheptadecatrienoic acid, a BLT2 ligand. *J Lipid Res.* 2013;54(11):2979-2987.

92. Okuno T, Gijon MA, Zarini S, Martin SA, Barkley RM, Johnson CA, Ohba M, Yokomizo T, and Murphy RC. Altered eicosanoid production and phospholipid remodeling during cell culture. *J Lipid Res.* 2018;59(3):542-549.

93. Sasaki F, Koga T, Saeki K, Okuno T, Kazuno S, Fujimura T, Ohkawa Y, and Yokomizo T. Biochemical and immunological characterization of a novel monoclonal antibody against mouse leukotriene B4 receptor 1. *PLoS One.* 2017;12(9):e0185133.

891 94. Tsutsumi-Miyahara C, Sonoda KH, Egashira K, Ishibashi M, Qiao H, Oshima T,
892 Murata T, Miyazaki M, Charo IF, Hamano S, et al. The relative contributions of
893 each subset of ocular infiltrated cells in experimental choroidal
894 neovascularisation. *Br J Ophthalmol.* 2004;88(9):1217-1222.
895 95. Ichiki T, Koga T, Okuno T, Saeki K, Yamamoto Y, Yamamoto H, Sakaguchi M,
896 and Yokomizo T. Modulation of leukotriene B4 receptor 1 signaling by receptor
897 for advanced glycation end products (RAGE). *FASEB J.* 2016;30(5):1811-1822.

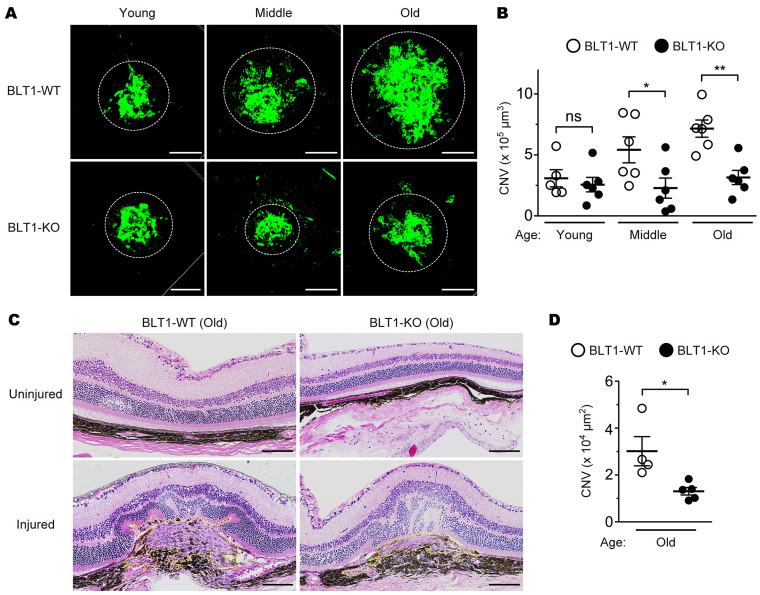

898 **Figure 1. BLT1 deficiency attenuates CNV in a mouse model of AMD.**
899 Images of isolectin B4 (iB4) staining (A) and CNV volume (B) in the RPE-choroid
900 complex from the eyes of BLT1-WT (open circles) and BLT1-KO (filled circles) mice
901 after laser-induced injury. Green represents a CNV area positive for iB4 staining. Mice
902 were grouped by age: Young, 8–12 weeks old; Middle-aged, 20–24 weeks old; Old, 40–
903 48 weeks old. *n*=5–6 mice per group. (C, D) H&E staining of the uninjured and laser-
904 injured retinas from aged BLT1-WT and BLT1-KO mice (> 40 weeks old). Yellow dotted
905 lines denote the lesion areas. *n*=4–5 per group. Bar=100 µm (A, C). (B, D) **P* < 0.05;
906 ***P* < 0.01; ns, not significant (1-way ANOVA with Bonferroni's *post hoc* test [B] and
907 Student's *t* test [D]). Results are representative of at least two independent experiments.

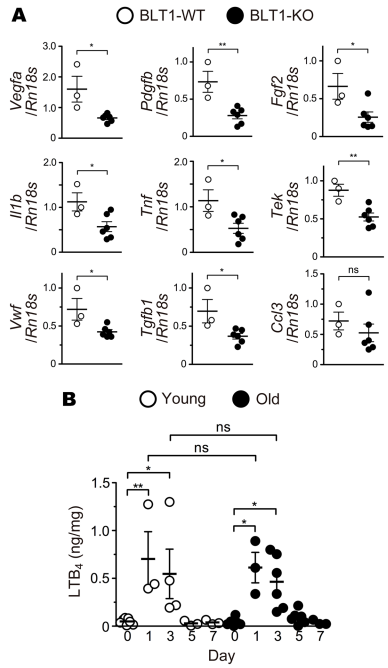

908 Figure 2. BLT1 deficiency reduces expression of pro-angiogenic and pro-fibrotic
909 factors in the laser-induced eyes.
910 (A) Quantitative RT-PCR analysis of mRNA for various pro-angiogenic and pro-fibrotic
911 factors, cytokines, and chemokines in the eyes from aged BLT1-WT (white bars) and
912 BLT1-KO (black bars) mice (> 20 weeks old) on Day 7 post-laser injury. *n*=3–6 per group.
913 (B) Time-dependent changes in LTB_4 content in laser-injured eyes from young (white
914 bars) and old (black bars) WT mice (Young, 8 weeks old; Old, > 20 weeks old). *n*=3–7
915 per group. (A, B) $*P < 0.05$; $**P < 0.01$; ns, not significant (Student's *t* test [A] and 1-
916 way ANOVA with Bonferroni's *post hoc* test [B]). Results are representative of at least
917 two independent experiments.

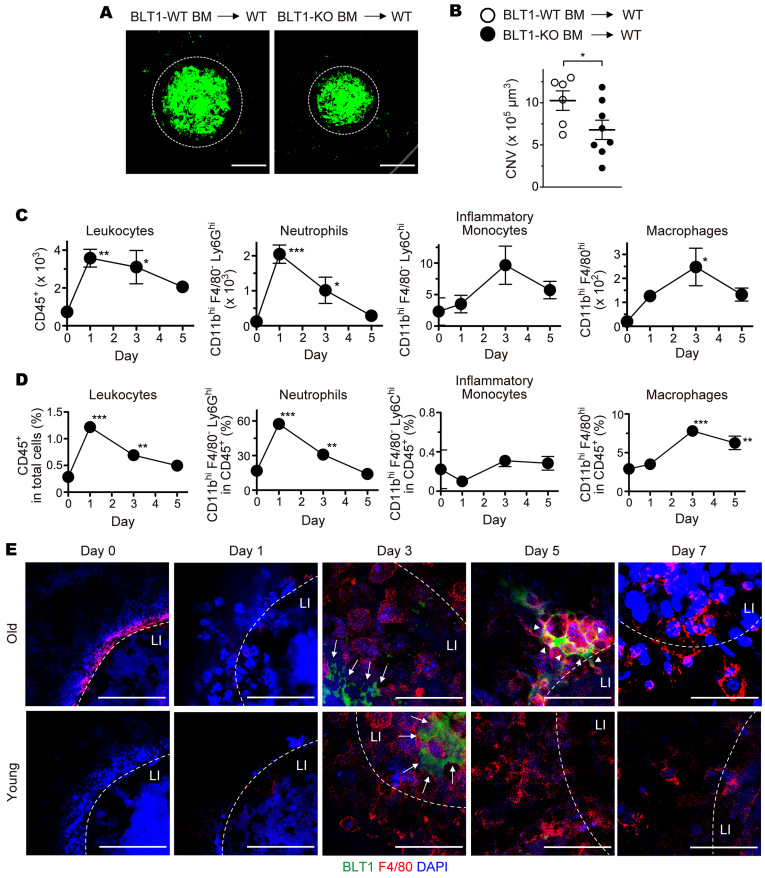

Figure 3. BLT1-expressing macrophages are recruited to the periphery of laser-induced CNV.

Images of iB4 staining (A) and CNV volume (B) in the RPE-choroid of chimeric mice receiving BM cells from aged BLT1-WT (open circles) or BLT1-KO (filled circles) mice (> 20 weeks old). *n*=6–8 mice per group. (C, D) FACS analysis of cells isolated from the laser-injured eyes of aged WT mice (> 20 weeks old). The populations of the leukocytes are gated as follows: total leukocytes: $CD45^+$, neutrophils: $CD11b^{hi}$ $F4/80^-$ $Ly6G^+$, inflammatory monocytes: $CD11b^{hi}$ $F4/80^-$ $Ly6C^+$, macrophages: $CD11b^{hi}$ $F4/80^{hi}$. The numbers (C) and percentages (D) of the leukocyte populations were analyzed on Day 1, Day 3, and Day 5 post-laser injury. Day 0 refers to a sample taken from uninjured eyes. *n*=3–4 per group. (E) Immunofluorescence staining of the laser-injured RPE-choroids from WT mice (Young, 8 weeks old; Old, > 20 weeks old) with anti-F4/80 (red) and -BLT1 (green) mAbs. Nuclei were visualized with DAPI (blue). LI (white dotted lines) denotes the location of laser injury. White arrows show F4/80-negative and BLT1-positive cells. White arrowheads show F4/80- and BLT1-double positive cells. Bar=100 µm (A) or 50 µm (E). (B) $*P < 0.05$ (Student's *t* test). (C, D) $*P < 0.05$; $**P < 0.01$; $***P < 0.005$ versus Day 0 (1-way ANOVA with Dunnett's *post hoc* test). Results are representative of at least two independent experiments.

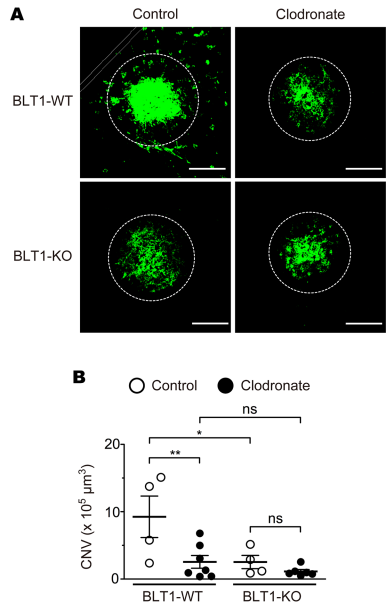

Figure 4. BLT1-expressing macrophages are involved in the pathogenesis of laser-induced CNV.

(A, B) The effect of clodronate liposome-mediated macrophage depletion (indicated as "Clodronate", filled circles) on CNV volume in aged BLT1-WT and BLT1-KO mice (> 20 weeks old). "Control" refers to control liposomes (open circles). n=4–7 mice per group. Bar=100 µm. (B) *$P < 0.05$; **$P < 0.01$; ns, not significant (1-way ANOVA with Newman-Keuls *post hoc* test). Results are representative of at least two independent experiments.

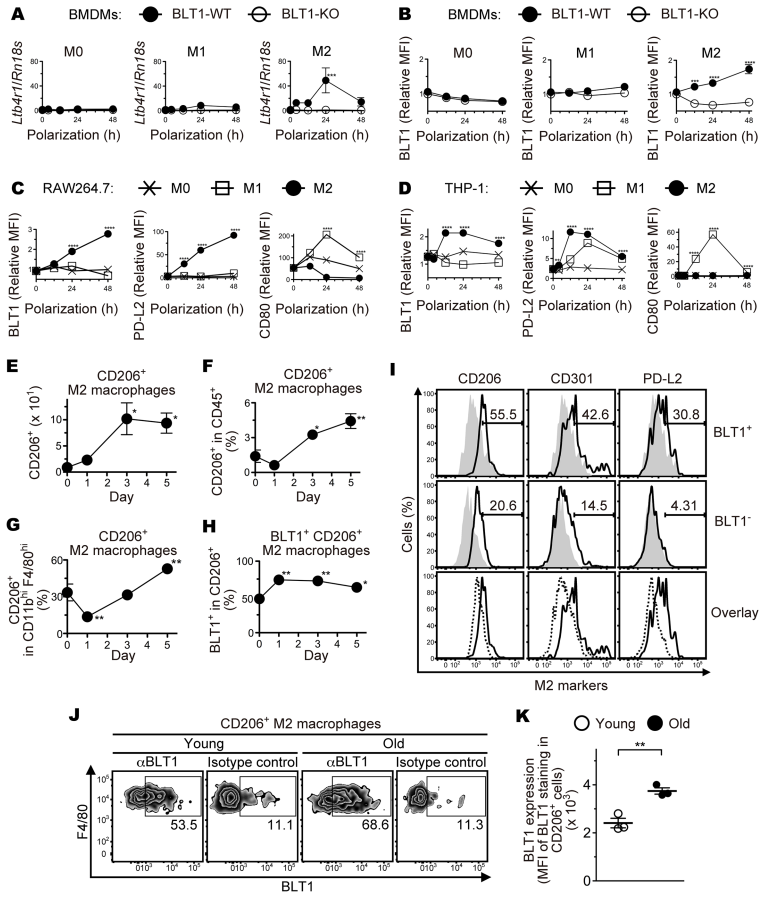

Figure 5. M2-type macrophages express BLT1 and infiltrates into the injured eyes of aged mice.

BMDMs from aged BLT1-WT (filled circles) and BLT1-KO (open circles) mice (> 20 weeks old) were polarized to M1 and M2 macrophages, and BLT1 expression was examined by quantitative RT-PCR (A) and FACS analysis (B). M0 denotes a sample of non-polarized BMDMs. RAW264.7 (C) and THP-1 (D) cells were polarized to M0 (cross plots), M1 (open squares), and M2 (filled circles) macrophages, and expression of BLT1, PD-L2 (an M2 marker), and CD80 (an M1 marker) was examined by flow cytometry. The Y-axis shows the MFI relative to that of an isotype control (mouse IgG_1). MFI, mean fluorescence intensity. *n*=3 per group. (E, F, G, H) FACS analysis of M2 macrophages isolated from the laser-injured eyes of aged WT mice (> 20 weeks old) as described in Figure 3C and D. $CD206^+$ M2 macrophages: $CD11b^{hi}$ $F4/80^{hi}$ $CD206^+$, $CD206^+$ $BLT1^+$ M2 macrophages: $CD11b^{hi}$ $F4/80^{hi}$ $CD206^+$ $BLT1^+$. *n*=3–4 per group. (I) FACS analysis of M2 markers on the ocular-infiltrating $BLT1^+$ and $BLT1^-$ macrophages on Day 5 post-laser injury from aged WT mice. CD206, CD301, and PD-L2 are specific surface markers of M2 macrophages. Cells were stained with anti-CD206, anti-CD301, and anti-PD-L2 mAbs (black outlines) or isotype controls (gray filled histograms). Overlays show the expression level of M2 markers on $BLT1^+$ (black outlines) and $BLT1^-$ (black dotted lines) macrophages. These macrophages were gated as the $CD45^+$ $F4/80^{hi}$ $CD11b^{hi}$ population. (J, K) FACS analysis of BLT1 expression on the ocular-infiltrating $CD206^+$ M2 macrophages on Day 3 post-laser injury from young or aged WT mice. *n*=3 per group. (A, B, C, D) $^{**}P < 0.01$; $^{***}P < 0.005$; $^{****}P < 0.001$ versus 0 h (2-way ANOVA with Bonferroni's *post hoc* test). (E, F, G, H) $^{*}P < 0.05$; $^{**}P < 0.01$ versus Day 0 (1-way

ANOVA with Dunnett's *post hoc* test). (K) $^{**}P < 0.01$ (Student's *t* test). Results are representative of at least two independent experiments (A-I).

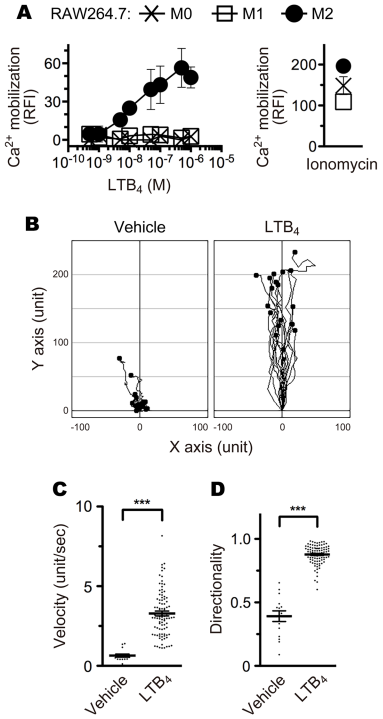

969 **Figure 6. M2 macrophages respond to LTB_4.**
970 (A) Calcium mobilization in M0- (cross plots), M1- (open squares), and M2- (filled
971 circles) RAW264.7 cells after stimulation with the indicated concentrations of LTB_4 and
972 2 μM ionomycin. *n*=3 per group. (B) Chemotaxis of M2-RAW264.7 cells toward 100 nM
973 (highest concentration) of LTB_4 (*n*=18) or vehicle (*n*=15). The velocity (C) and
974 directionality (D) of M2-RAW264.7 cell migration in the presence of vehicle (*n*=15) or
975 100 nM LTB_4 (*n*=93) are shown. (C, D) ***$P < 0.005$ (Student's *t* test). Results are
976 representative of at least two independent experiments.

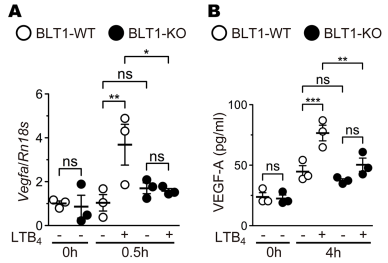

977 **Figure 7. LTB_4-BLT1 signaling induces VEGF-A production in M2 macrophages.**
978 BMDMs from aged BLT1-WT (open bars) and BLT1-KO (filled bars) mice (> 20 weeks
979 old) were polarized to M2 macrophages, and were stimulated with 500 nM LTB_4 or
980 vehicle for 0.5 h (A) or 4 h (B). The expression levels of VEGF-A mRNA (A) and protein
981 (B) were measured by quantitative RT-PCR and ELISA. n=3 per group. (A, B) *$P < 0.05$;
982 **$P < 0.01$; ***$P < 0.005$; ns, not significant (1-way ANOVA with Newman-Keuls *post*
983 *hoc* test). Results are representative of at least two independent experiments.

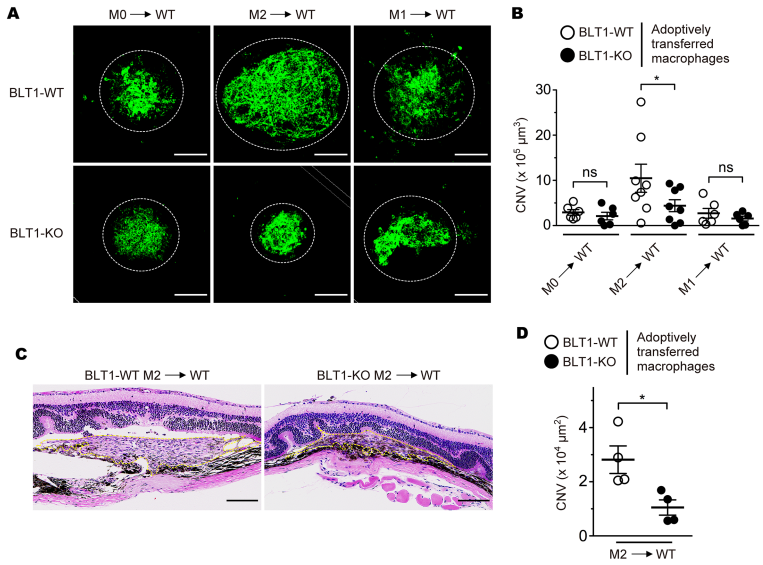

Figure 8. M2 macrophage-dependent CNV development requires BLT1.
Images of iB4 staining (A) and CNV volume (B) in the RPE-choroid of recipient mice that received M0-, M2-, and M1-BMDMs from aged BLT1-WT (open circles) or BLT1-KO (filled circles) mice (> 20 weeks old). *n*=6–8 mice per group. (C, D) H&E staining of the laser-injured retinas of recipient mice receiving M2-BMDMs from BLT1-WT or BLT1-KO mice (> 20 weeks old). Yellow dotted lines show the lesion area. *n*=4 per group. Bar=100 µm (A, C). (B, D) **P* < 0.05; ns, not significant (1-way ANOVA with Bonferroni's *post hoc* test [B] and Student's *t* test [D]). Results are representative of at least two independent experiments.

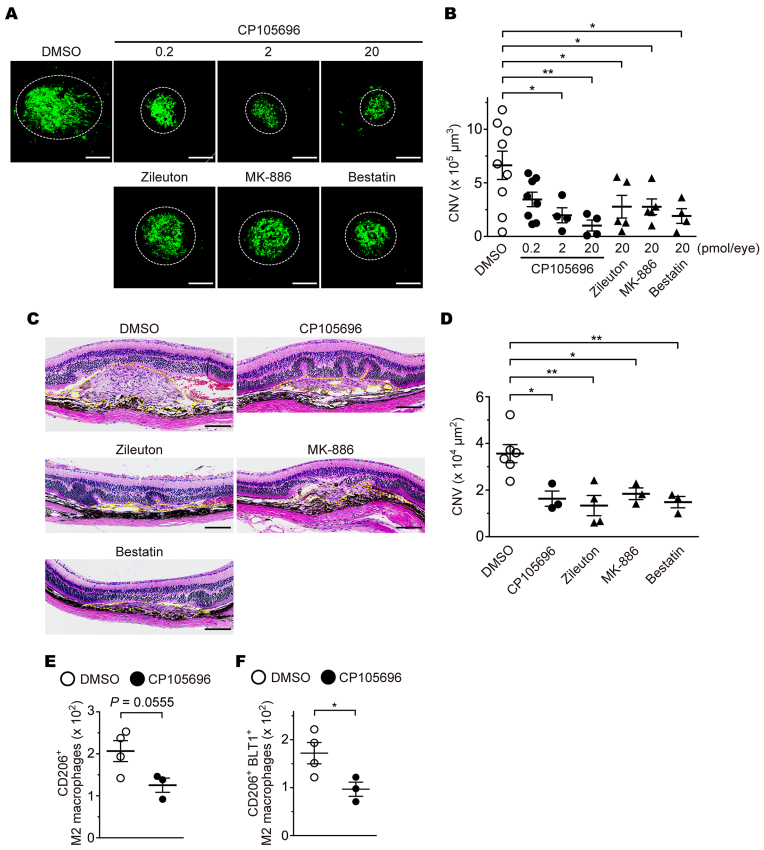

Figure 9. The effects of a BLT1 antagonist and LTB_4 synthesis inhibitors on development of CNV.

Images of iB4 staining (A) and CNV volume (B) in the RPE-choroid from aged WT mice (> 20 weeks old) after administration of 0.2–20 pmol of CP105696 (a BLT1 antagonist; filled circles) or 20 pmol of Zileuton (a 5-LO inhibitor), MK-886 (a FLAP inhibitor), or Bestatin (a LTA_4H inhibitor) (filled triangles), or vehicle (open circles). *n*=4–9 mice per group. (C, D) H&E staining of the retinas after aged WT mice (> 20 weeks old) with laser-induced injury were treated with CP105696, Zileuton, MK-886, and Bestatin (20 pmol/eye), or DMSO. Yellow dotted lines show the lesion area. *n*=3-6 per group. (E, F) The number of the ocular-infiltrating $CD206^+$ or $CD206^+$ $BLT1^+$ M2 macrophages was analyzed on Day 3 post-laser injury from CP105696- (20 pmol/eye) or DMSO-injected WT mice (> 20 weeks old). *n*=3-4 per group. Bar=100 μm (A, C). (B, D) $*P < 0.05$; $**P < 0.01$ (1-way ANOVA with Dunnett's *post hoc* test [B, D] and Student's *t* test [E, F]). Results are representative of at least two independent experiments (A-D).